Research Article | Vol. 27, No. 3 | 4 Feb 2019 | OPTICS EXPRESS 3717
Optics EXPRESS

Calculation of the impulse response and phase noise of a high-current photodetector using the drift-diffusion equations

SEYED EHSAN JAMALI MAHABADI,[1,*] SHAOKANG WANG,[1] THOMAS F. CARRUTHERS,[1] CURTIS R. MENYUK,[1] FRANKLYN J. QUINLAN,[2] MEREDITH N. HUTCHINSON,[3] JASON D. MCKINNEY,[3] AND KEITH J. WILLIAMS[3]

[1]*Department of Computer Science and Electrical Engineering, University of Maryland, Baltimore County, Baltimore, MD 21250, USA*
[2]*National Institute of Standards and Technology, Boulder, Colorado 80305, USA*
[3]*U.S. Naval Research Laboratory, Washington, DC 20375, USA*
[*]*sjamali1@umbc.edu*

Abstract: We describe a procedure to calculate the impulse response and phase noise of high-current photodetectors using the drift-diffusion equations while avoiding computationally expensive Monte Carlo simulations. We apply this procedure to a modified uni-traveling-carrier (MUTC) photodetector. In our approach, we first use the full drift-diffusion equations to calculate the steady-state photodetector parameters. We then perturb the generation rate as a function of time to calculate the impulse response. We next calculate the fundamental shot noise limit and cut-off frequency of the device. We find the contributions of the electron, hole, and displacement currents. We calculate the phase noise of an MUTC photodetector. We find good agreement with experimental and Monte Carlo simulation results. We show that phase noise is minimized by having an impulse response with a tail that is as small as possible. Since, our approach is much faster computationally than Monte Carlo simulations, we are able to carry out a broad parameter study to optimize the device performance. We propose a new optimized structure with less phase noise and reduced nonlinearity.

1. Introduction

Phase noise in the photodetectors is a critical limiting factor in many RF-photonic applications [1, 2], particularly in metrology applications in which excess phase noise inherent in the photodetection process limits the extent to which the low noise of an optical pulse train from an optical frequency comb can be transferred to the microwave domain [2]. The standard approach to calculate white phase noise floor and the cut-off frequency in a photodetector is to find the impulse response of the individual electrons that are created in response to the Poisson-distributed incoming light and the efficiency with which they are created [1, 3]. The resulting fluctuations in the timing of the impulses manifest themselves as phase noise on the microwave harmonics of the optical pulse repetition frequency [4–6]. This approach must be modified in a high-current photodetector, in which space charge effects due to the large number of carriers in the device affect the impulse response and the carrier fluctuations. Quinlan *et al*. [3] theoretically predicted that the phase noise from a train of ultrashort optical pulses becomes lower and tends to zero as the optical pulse duration tends to zero. Later experiments showed that while there is a significant reduction in the phase noise as the pulse duration decreases, this decrease in the phase noise ceases once the optical pulse duration becomes small compared to the duration of the electrical pulse that emerges from the photodetector [7]. Sun *et al*. [8] were able to reproduce these experimental results using Monte Carlo simulations that accounted for collisional diffusion of electrons in the device. However, they did not take advantage of the fact that the distribution of electrons in any time slot is expected to be Poissonian, which simplifies both the calculations and

#349893 https://doi.org/10.1364/OE.27.003717
Journal © 2019 Received 2 Nov 2018; revised 21 Dec 2018; accepted 3 Jan 2019; published 1 Feb 2019

Optics EXPRESS

the physical interpretation of the results. More practically, the Monte Carlo simulations are too computationally slow to be used for performance optimization.

Here, we use the drift-diffusion equations [9, 10], combined with the observation that the arrival of electrons in any time interval is Poisson-distributed, to calculate the phase noise. This approach takes minutes on a desktop computer, as opposed to the many hours on a computer cluster that the Monte Carlo approach requires. We explain analytically that the mean-square phase noise tends to a constant non-zero value when the optical pulse duration tends to zero. Finally, we use our approach to study how the device parameters affect the phase noise and optimize the performance. In our approach, we treat the incoming light as a time-dependent field with a variation about its mean at any time that is determined by the Poisson distribution of the photons. We apply this approach to a modified uni-traveling-carrier (MUTC) photodetector, a device in which photogenerated holes are prevented from moving by potential barriers, so that electrons dominate the photocurrent [11]. We compare our calculated impulse response to the response that was obtained earlier using Monte Carlo simulations [8], and we find good agreement. We next show that the quantum efficiency of the device with an input light pulse is the same as the steady-state quantum efficiency of the device, and we calculate the shot noise level, which is also in good agreement with experiments [7]. We also calculate the cut-off frequency of the device using the 3-dB roll-off in the impulse response. Finally we calculate the phase noise for the device. In the simulation, we use the device parameters that were used by Sun *et al*. [8] We set the output current, I_{out}, equal to 15 mA, we set the bias voltage, V_{bias}, equal to 16 V, we set the external load impedance, R_{load}, equal to 50 Ω, and we set the MUTC photodetector diameter equal to 50 μm. Figure 1 shows the structure of the MUTC photodetector [7, 8, 11].

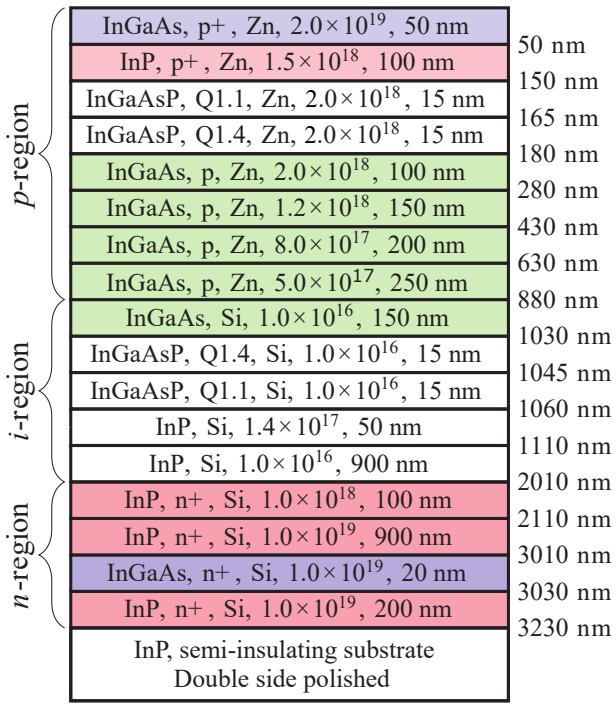

Fig. 1. Structure of the MUTC photodetector. Green indicates the absorption layers, which include an intrinsic region and a p-doped region. Red indicates highly doped InP layers, purple indicates highly-doped InGaAs layers, and white indicates other layers.

Optics EXPRESS

2. 1-D computational model

We use a one-dimensional (1-D) model of the MUTC photodetector [9, 10] to calculate the impulse response of the device. External loading, impact ionization, and the Franz-Keldysh effect are all considered in the simulations. We review our 1-D computational model in Appendix A.

To calculate the impulse response, we first calculate the steady state output current. We then perturb the generation rate by ΔG_{opt} for a small time starting at $t = 0$ and calculate the impulse response due to the perturbed ΔG_{opt}. We use

$$\Delta G_{\text{opt}} = r G_{\text{opt}} \,\text{rect}\left(\frac{t}{\tau}\right), \tag{1}$$

where G_{opt} is the optical generation rate, r is the perturbation coefficient, $\text{rect}(t)$ is the rectangular function

$$\text{rect}(t) = \begin{cases} 0, & t < 0 \\ 1, & 0 < t < 1 \\ 0, & 1 < t \end{cases}$$

and t is time. We set $\tau = 10$ fs, which we verified produces reliable results for the impulse response for times that are larger than 40 fs. We use $r = 10^{-1}$, which we have verified is sufficiently small that no nonlinear effects occur, while it is large enough to avoid roundoff errors. While it is possible in principle to linearize drift-diffusion equations about the stationary solution and solve the linearized equations to obtain the impulse response, the equations that we obtain with this direct linearization are sufficiently complex that there is no advantage in doing so. The normalized impulse response $h(t)$ is then given by

$$h(t) = \frac{\Delta I_{\text{out}}(t)}{\int_0^\infty \Delta I_{\text{out}}(t)\, \text{d}t}, \tag{2}$$

so that $\int_0^\infty h(t)dt = 1$, where $\Delta I_{\text{out}}(t)$ is the change in the output current due to the impulse.

We note that $h(t)$ as defined here includes the combined effect of a finite optical pulse duration and the electrical response to that pulse. This definition is consistent with the one of Quinlan *et al*. [3] and Sun *et al*. [8] In order to verify that our results are independent of the choice of τ and r, we ran numerical tests in which we allowed these quantities to vary.

3. Results

In this section, we present the results for the MUTC photodetector. We also compare the impulse response of the MUTC photodetector to the results of Sun *et al*. [8] In Fig. 2, we show the electric field and carrier distributions at steady state inside the MUTC photodetector. Electron-hole pairs are created inside the region shown as vertical dot-dashed lines. Holes are rapidly absorbed in the p-contact region, while electrons move to the intrinsic region, where they experience a strong electric field before moving to the n-region, where they diffuse to the n-contact. Holes do not contribute significantly to the total current as active carriers due to the position of the absorption layers. In an MUTC photodetector, the only absorption layers are in the p-region. The intrinsic region only contains collection layers. Photogenerated majority holes diffuse almost immediately to the p-contact. There is a diffusion blocking layer on the left side of the absorption layers that prevents electrons from diffusing to the p-contact [12]. In Fig. 3, we show the normalized impulse response of the MUTC photodetector as a function of time. In contrast to a PIN photodetector [13], the displacement current cannot be neglected, and it dominates the total current for the first 50 fs. Thereafter, the electron current dominates at all times, in sharp contrast to the PIN photodetector described by Hu *et al*. [9] for which the hole current dominates beyond 70 fs. The total current of the MUTC photodetector is sum of the electron, hole, and

Optics EXPRESS

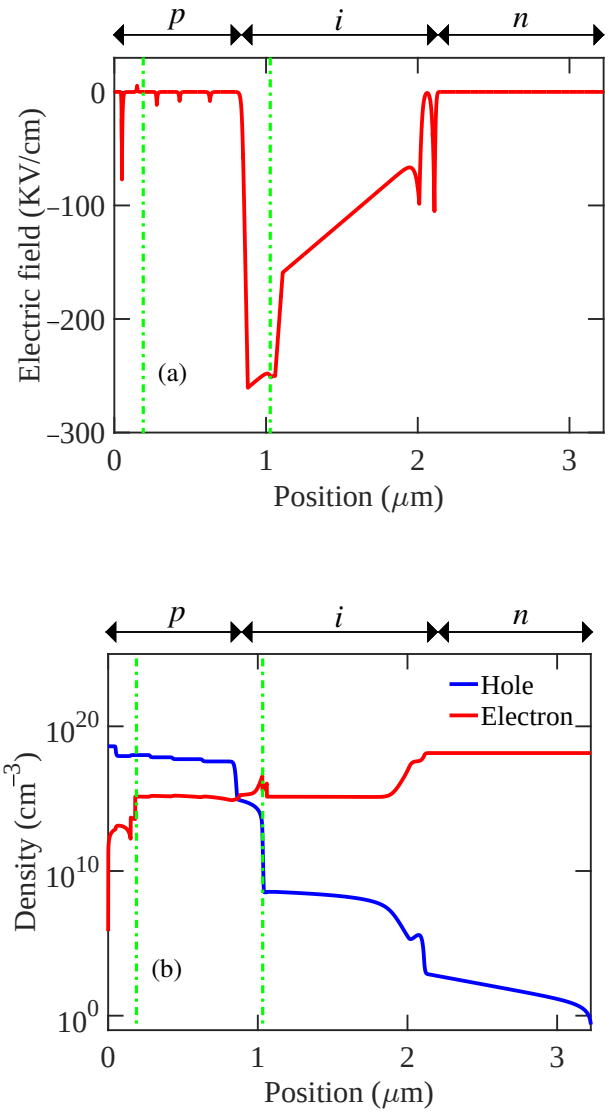

Fig. 2. (a) Electric field distribution at steady state inside the MUTC photodetector and (b) density of electrons (red) and holes (blue) at steady state inside the MUTC photodetector. I_{out} = 15 mA and V_{bias} = 16 V. The photon absorption region is shown between vertical dot-dashed lines.

displacement currents. The displacement current dominates the total current for the first 50 fs and is negative. Beyond 70 fs, electrons dominate the total current, and it becomes positive.

Figure 4 shows the power spectral density $|H(f)|^2$, where $H(f)$ is the transfer function of the

Optics EXPRESS

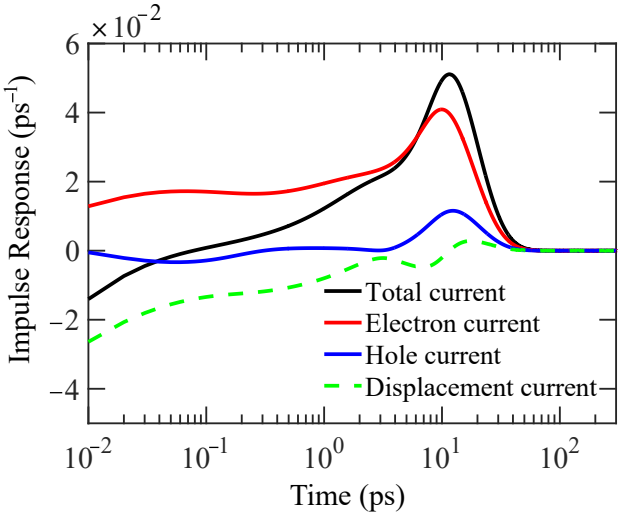

Fig. 3. Normalized impulse response of the MUTC photodetector.

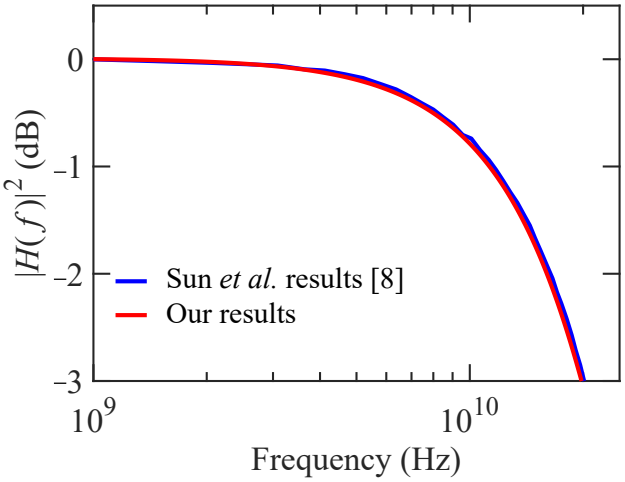

Fig. 4. Power spectral density of the MUTC photodetector.

photodetector, defined as

$$H(f) = \int_{-\infty}^{\infty} h(t) \exp(-2\pi j f t)\, dt. \tag{3}$$

and we used square pulses that are defined in Eq. (1). We compare this result to an average of the power spectral density that Sun *et al*. [8] reported from five realizations of their Monte Carlo simulations. They computed their power spectral density using an impulse with a duration of 15 ps. We computed $h(t)$ and $|H(f)|^2$ using an impulse duration of 15 ps with a peak output current of 130 mA, which corresponds to the results of Sun *et al*. [8] We have found that when the optical pulse duration is less than about 500 fs, the impulse response tends to a finite limit $h_e(t)$ that represents the electronic response and has a mean-square pulse duration ~ 90 ps^2 for the MUTC device that we are considering. We show the results in Fig. 4.

Optics EXPRESS

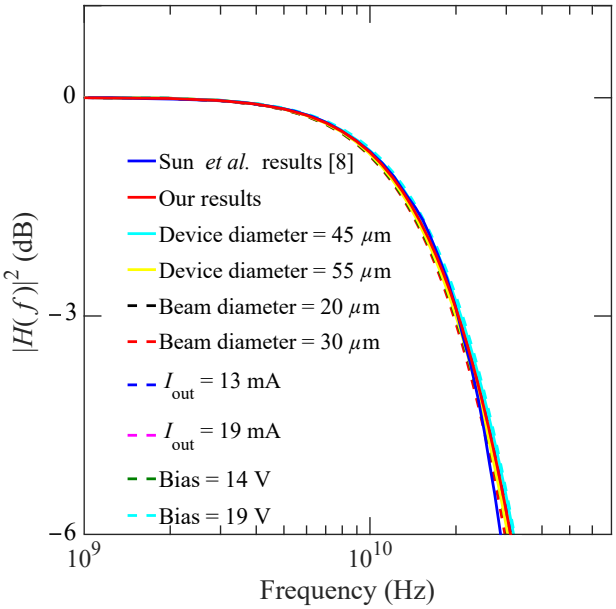

Fig. 5. Power spectral density of the MUTC photodetector for different parameters.

The calculation of the impulse response using the drift-diffusion equations is far more rapid computationally than is the calculation of the impulse response using Monte Carlo simulations. Hence, it is possible to do a broad parameter study. In Fig. 5, we compare the device diameter, beam diameter, steady state output current, and the voltage bias. We compare these results to the average of the power spectral density that Sun *et al*. [8] reported from five realizations of their Monte Carlo simulations. The bandwidth increases when the device diameter decreases [11], which we attribute to a decrease in capacitance. However, the difference is less than 2 GHz among all the cases that we considered.

For the device used by Quinlan *et al*. [7] and Sun *et al*. [8], we calculated a quantum efficiency of $\eta = 56\%$. We also calculated a 3-dB cut-off frequency of 20 GHz, which is consistent with the results of Sun *et al*. [8]

4. Phase noise in the MUTC photodetector

In this section we calculate the phase noise of the MUTC photodetector and compare our results to the Monte Carlo simulation results of Sun *et al*. [8] and to the experimental results of Quinlan *et al*. [7] We first calculate the timing jitter using the impulse response function, and we then use the timing jitter to calculate the phase noise.

We define the finite-time Fourier transform,

$$\mathscr{F}_T\{x(t)\} \equiv \int_{-T/2}^{T/2} x(t)\exp(-j2\pi ft)\,\mathrm{d}t. \tag{4}$$

Optics EXPRESS

We next write

$$\begin{aligned}\mathscr{F}_T\{i(t)\} &= \int_{-T/2}^{T/2} i(t)\exp(-j2\pi ft)\,\mathrm{d}t \\ &= \frac{1}{2K}\sum_{k=-K}^{K-1}\int_0^{T_R} i(t+kT_R)\exp[-j2\pi f(t+kT_R)]\,\mathrm{d}t,\end{aligned} \tag{5}$$

where $i(t)$ is the output current, T_R is the repetition time between optical pulses, and $T = KT_R$. If we let $i_k(t) = i(t + kT_R)$, so that $i_k(t)$ is the k-th current output pulse, we obtain

$$\mathscr{F}_T\{i(t)\} = \frac{1}{2K}\sum_{k=-K}^{K-1}\int_0^{T_R} i_k(t)\exp(-j2\pi ft)\,\mathrm{d}t. \tag{6}$$

For the n-th harmonic of the current, we obtain

$$R_n + jQ_n = \frac{1}{2K}\sum_{k=-K}^{K-1}\int_0^{T_R} i_k(t)\left[\cos(2\pi nf_rt) - j\sin(2\pi nf_rt)\right]\,\mathrm{d}t, \tag{7}$$

where R_n and Q_n are in-phase and quadrature components of the n-th harmonic. We also define the ensemble average $\langle c_k(t)\rangle$ for any quantity $c_k(t)$ as

$$\langle c_k(t)\rangle \equiv \lim_{K\to\infty}\frac{1}{2K}\sum_{k=-K}^{K-1} c_k(t). \tag{8}$$

It is useful to shift the time to remove the quadrature component to good approximation. To do that, we write

$$R_n + jQ_n = \frac{1}{2K}\sum_{k=-K}^{K-1}\int_0^{T_R} i_k(t)\left\{\cos\left[\frac{2\pi n}{T_R}(t-t_c)\right] - j\sin\left[\frac{2\pi n}{T_R}(t-t_c)\right]\right\}\mathrm{d}t, \tag{9}$$

where t_c is central time of the output current, which is implicitly defined by the relation

$$Q_n = \int_0^{T_R}\langle i_k(t)\rangle\sin\left[\frac{2\pi n}{T_R}(t-t_c)\right]\mathrm{d}t = 0. \tag{10}$$

We next define

$$\Phi_n = \frac{-j\sum_{k=-K}^{K-1}\int_0^{T_R} i_k(t)\sin\left[\frac{2\pi n}{T_R}(t-t_c)\right]\mathrm{d}t}{\sum_{k=-K}^{K-1}\int_0^{T_R} i_k(t)\cos\left[\frac{2\pi n}{T_R}(t-t_c)\right]\mathrm{d}t} = 0. \tag{11}$$

Although we have $\Phi_n = 0$, the separate phase contributions of each comb pulse to Φ_n will be non-zero. We have $\Phi_n = \sum_k \Phi_{kn}$ and $Q_n = \sum_k Q_{kn}$, where

Optics EXPRESS

$$\Phi_{kn} = \frac{Q_{kn}}{R_n} = \frac{-j\int_0^{T_R} i_k(t)\sin\left[\frac{2\pi n}{T_R}(t-t_c)\right]\mathrm{d}t}{\int_0^{T_R} i_k(t)\cos\left[\frac{2\pi n}{T_R}(t-t_c)\right]\mathrm{d}t}. \tag{12}$$

We next find

$$\Phi_{kn}^2 = \frac{\int_0^{T_R}\int_0^{T_R} i_k(t)i_k(u)\sin\left[\frac{2\pi n}{T_R}(t-t_c)\right]\sin\left[\frac{2\pi n}{T_R}(u-t_c)\right]\mathrm{d}t\mathrm{d}u}{\left\{\int_0^{T_R} i_k(t)\cos\left[\frac{2\pi n}{T_R}(t-t_c)\right]\mathrm{d}t\right\}^2}. \tag{13}$$

We may assume that the electrons in each current pulse are Poisson-distributed. This assumption may seem surprising at first since the photodetectors of interest to us operate in a nonlinear regime. However, the electrons only interact through the electric field that they collectively create. Due to the large number of electrons that create this field, a mean-field approximation is valid, and the arrival time of the electrons is nearly independent. Given the assumption that the current pulses are Poisson-distributed, we find

$$\langle i_k(t)i_k(u)\rangle - \langle i_k(t)\rangle\langle i_k(u)\rangle = h(t)e^2N_{\mathrm{tot}}\delta(t-u). \tag{14}$$

Taking the ensemble average of Eq. (13), substituting Eq. (15) into this ensemble-averaged equation, and using Eq. (10), we find

$$\left\langle\Phi_n^2\right\rangle = \frac{1}{N_{\mathrm{tot}}}\frac{\int_0^{T_R} h(t)\sin^2\left[2\pi n(t-t_c)/T_R\right]\mathrm{d}t}{\left\{\int_0^{T_R} h(t)\cos\left[2\pi n(t-t_c)/T_R\right]\mathrm{d}t\right\}^2}, \tag{15}$$

where $\left\langle\Phi_n^2\right\rangle$ is the mean-square phase fluctuation and N_{tot} is the total number of electrons in the photocurrent. Increasing the photocurrent for a given impulse response $h(t)$ decreases the phase noise. In the limit of short optical pulse durations ($\lesssim$ 500 fs), we find that $\langle\Phi_n^2\rangle$ tends to a non-zero constant, which is given by

$$\left\langle\Phi_n^2\right\rangle = \frac{1}{N_{\mathrm{tot}}}\frac{\int_0^{T_R} h_e(t)\sin^2\left[2\pi n(t-t_c)/T_R\right]\mathrm{d}t}{\left\{\int_0^{T_R} h_e(t)\cos\left[2\pi n(t-t_c)/T_R\right]\mathrm{d}t\right\}^2}, \tag{16}$$

where $h_e(t)$ is the electronic impulse response of the device. From Eq. (16), we infer that pulse noise is reduced for a fixed pulse energy by designing the photodetector so that its impulse response is as close to square as possible. We stress that this analysis applies to any photodetector, not only MUTC photodetectors.

Using Eq. (16), we calculate the phase noise of the MUTC photodetector. Figure 6 shows the phase noise of the MUTC photodetector as a function of offset frequency from the fifth harmonic at 10 GHz for three different optical pulse widths. We show the phase noise deviation from the long pulse limit as a function of the optical pulse width in Fig. 7.

Optics EXPRESS

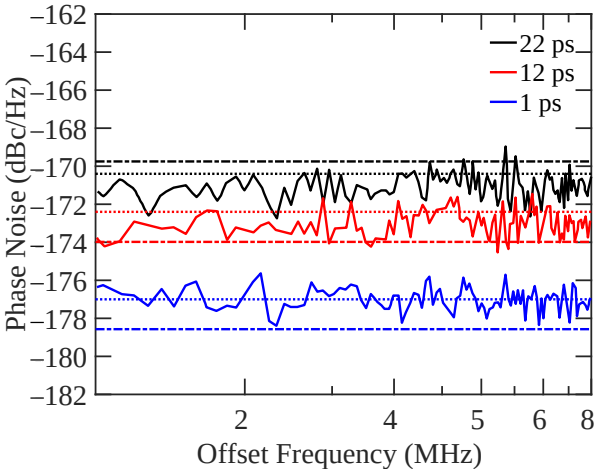

Fig. 6. Phase noise of the MUTC photodetector as a function of offset frequency from the fifth harmonic at 10 GHz for three different optical pulse widths. Dot-dashed lines are experimental results of Quinlan *et al*. [7]; solid lines are Monte Carlo simulation results of Sun *et al*. [8]; dotted lines are our simulation results.

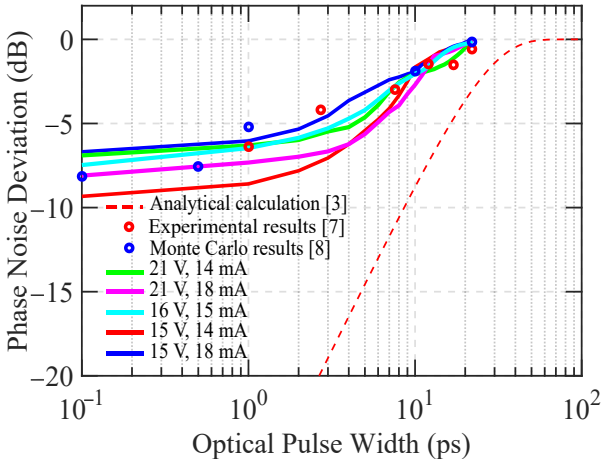

Fig. 7. Phase noise deviation from the long pulse limit.

As shown in Figs. 6 and 7, we obtain good agreement with both experimental and Monte Carlo simulation results. Here, we considered a range of average currents between 14 mA and 18 mA and bias voltages between 15 V and 21 V, which correspond to the ranges in the experiments of Quinlan *et al*. [7] In Fig. 7, we show how the phase noise deviation from the long-pulse limit depends on the bias voltage and output current for the MUTC device considered earlier by Quinlan *et al*. [7] and Sun *et al*. [8] The computational rapidity of our approach makes it possible to carry out a detailed device optimization in which all the layer elements in the MUTC device are varied in order to minimize the phase noise while maintaining low nonlinearity, as described in the next section.

Optics EXPRESS

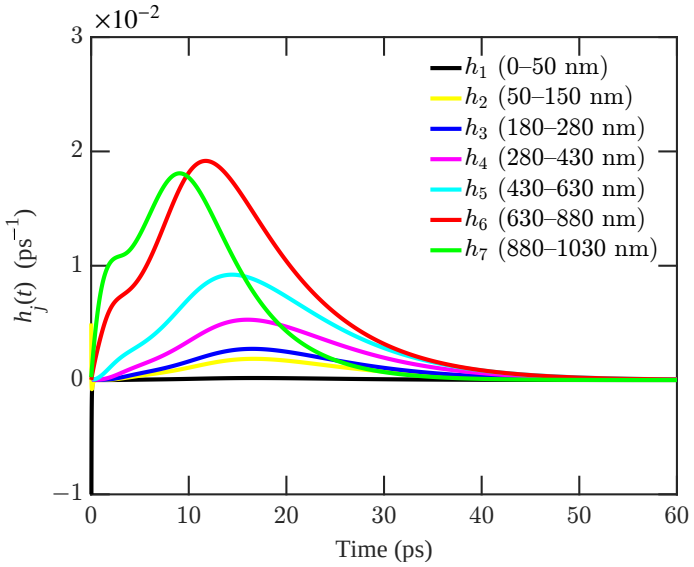

Fig. 8. Contribution of each of the absorption layers to the impulse response of the MUTC photodetector.

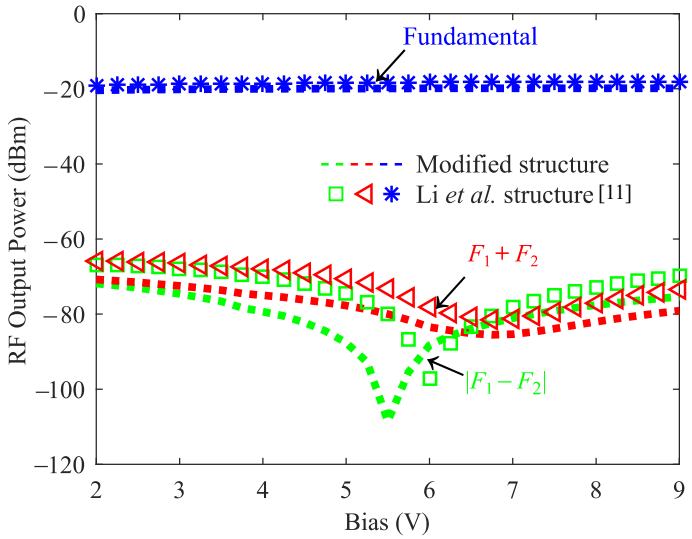

Fig. 9. Fundamental and IMD2 powers as a function of reverse bias for input frequencies F_1 = 4.9 GHz, F_2 = 5.0 GHz, and F_3 = 5.15 GHz for the Li *et al*. [11] structure and the modified structure.

5. Device optimization

Here, we use our approach to design an MUTC structure, based on the structure of Fig. 1, but with lower phase noise and nonlinearity. A long tail in the impulse response translates to higher phase noise. We performed a local optimization in which we modified the absorption layers to decrease the length of the tail in the impulse response and to lower the phase noise. In our optimization, we first altered the thickness of each of the absorption layers by up to 10%. However, we did not find a significant change in the impulse response. Next, we altered the doping density in

Optics EXPRESS

Table 1. Phase Noise 1 = phase noise of the Li *et al*. [11] structure; Phase Noise 2 = phase noise of the modified structure; Difference = (Phase Noise 1) − (Phase Noise 2).

Pulse Duration	Original structure	Modified structure	Difference
1 ps	−178.6 dBc/Hz	−180.0 dBc/Hz	1.4 dBc/Hz
12 ps	−174.0 dBc/Hz	−175.5 dBc/Hz	1.5 dBc/Hz
22 ps	−169.7 dBc/Hz	−172.8 dBc/Hz	3.1 dBc/Hz

each of the absorption layers. The total impulse response $h(t)$ is given by the sum of the impulse responses of each of the absorption layers separately, so that

$$h_e(t) = \sum_{j=1}^{N} h_j(t), \tag{17}$$

where $h_j(t)$ denotes the individual contribution of each layer. For the structure in Fig. 1, we have $N = 7$, and we show $h_j(t)$ in Fig. 8, along with the location of each layer. From Eq. (7) we conclude that it is desirable to reduce the variance of $h_e(t)$ as much as possible. We obtained our best results when we increased the doping density in layer $j = 4$ (280 nm–430 nm) from 1.2×10^{18} cm^{-3} to 1.5×10^{18} cm^{-3}, we decreased the density in layer $j = 5$ (430 nm–630 nm) from 8.0×10^{17} cm^{-3} to 6.0×10^{17} cm^{-3}, and we decreased the doping density in layer $j = 6$ (630 nm–880 nm) from 5.0×10^{17} cm^{-3} to 1.5×10^{17} cm^{-3}. These changes have the effect of reducing the size of the tail of $h_e(t)$. In Table 1, we compare the phase noise that we calculated for the structure of Li *et al*. [11] (structure 1) and our modified structure (structure 2) for three different pulse durations at which the phase noise is experimentally measured. In all cases, the phase noise is reduced by at least 1.4 dB.

We also calculated the harmonic powers in the modified structure and compared them to the harmonic powers in the Li *et al*. [11] structure as shown in Fig. 9. We find that there is no tradeoff with nonlinearity. The modified structure has a lower second-order intermodulation distortion (IMD2). It is not obvious that both phase noise and nonlinearity will improve simultaneously. To minimize phase noise, it is desirable to have an impulse response with a tail that is as small as possible. To minimize nonlinearity, it is desirable to minimize the variation of the efficiency and mean-square impulse response as a function of the input pulse energy. These criteria are not equivalent.

6. Conclusion

We have demonstrated that it is possible to accurately calculate the impulse response and the shot noise for high current photodetectors using the drift-diffusion equations. We then used the impulse response of the device to calculate the phase noise in an MUTC photodetector. Agreement with prior experiments and Monte Carlo simulations is excellent. Our approach is computationally faster than Monte Carlo simulations by many orders of magnitude. Hence, this approach makes it possible to optimize the device parameters in order to reduce the phase noise. Using our method, we modified the design of Li *et al*. [11] to obtain a structure with at least 1.4 dBc/Hz lower phase noise and reduced nonlinearity.

Appendix A

Here, we provide details of our 1-D model of the MUTC photodetector [9, 14]. Our starting point is the electron and hole continuity equations and the Poisson equation,

Optics EXPRESS

$$\begin{aligned}\frac{\partial(p-N_A^-)}{\partial t} &= -\frac{1}{q}\nabla\cdot\mathbf{J}_p + G_{\text{ii}} + G_{\text{opt}} - R(n,p),\\ \frac{\partial(n-N_D^+)}{\partial t} &= +\frac{1}{q}\nabla\cdot\mathbf{J}_n + G_{\text{ii}} + G_{\text{opt}} - R(n,p),\\ \nabla\cdot\mathbf{E} &= \frac{q}{\epsilon}\left(n-p+N_A^- - N_D^+\right),\end{aligned} \tag{18}$$

where n is the electron density, p is the hole density, t is time, q is the unit of charge, $\mathbf{J}_n$ is the electron current density, $\mathbf{J}_p$ is the hole current density, R is the recombination rate, G_{ii} and G_{opt} are the impact ionization and optical generation rates, $\mathbf{E}$ is the electric field, ϵ is the permittivity of the semiconductor material, N_A^- is the ionized acceptor concentration, and N_D^+ is the ionized donor concentration. The electron and hole current densities are governed by the equations

$$\begin{aligned}\mathbf{J}_p &= qp\mathbf{v}_p(\mathbf{E}) - qD_p\nabla p,\\ \mathbf{J}_n &= qn\mathbf{v}_n(\mathbf{E}) + qD_n\nabla n,\end{aligned} \tag{19}$$

where $\mathbf{v}_n(\mathbf{E})$ and $\mathbf{v}_p(\mathbf{E})$ are the electric-field-dependent electron and hole drift velocities, respectively, D_n is the electron diffusion coefficient, and D_p is the hole diffusion coefficient. The optical generation rate in Eq. (18) is

$$G_{\text{opt}} = G_c\,\exp\left[-\alpha(L-x)\right], \tag{20}$$

where G_c and α are the generation rate coefficient and absorption coefficient, respectively, x is distance across the device, and L is the device length.

The impact ionization generation rate in Eq. (18) is

$$G_{\text{ii}} = \alpha_n\frac{|\mathbf{J}_n|}{q} + \alpha_p\frac{|\mathbf{J}_p|}{q}, \tag{21}$$

where α_n and α_p are the impact ionization coefficients of electrons and holes, respectively, which are given by

$$\alpha_n = A_n\cdot\exp\left[-\left(\frac{B_n}{|\mathbf{E}|}\right)^m\right], \tag{22}$$

and

$$\alpha_p = A_p\cdot\exp\left[-\left(\frac{B_p}{|\mathbf{E}|}\right)^m\right], \tag{23}$$

where A_n, B_n, A_p, and B_p are parameters of impact ionization [9]. We set $m = 1.03$.

The recombination rate in Eq. (18) is

$$R = \frac{np-n_i^2}{\tau_p(n+n_i)+\tau_n(p+n_i)}, \tag{24}$$

where τ_n, τ_p, and n_i are the electron and hole lifetimes and intrinsic carrier density respectively. In steady state, Eq. (18) becomes

$$\begin{aligned}0 &= -\frac{1}{q}\nabla\cdot\mathbf{J}_p + G_{\text{ii}} + G_{\text{opt}} - R(n,p),\\ 0 &= +\frac{1}{q}\nabla\cdot\mathbf{J}_n + G_{\text{ii}} + G_{\text{opt}} - R(n,p),\\ \nabla\cdot\mathbf{E} &= \frac{q}{\epsilon}\left(n-p+N_A^- - N_D^+\right).\end{aligned} \tag{25}$$

Optics EXPRESS

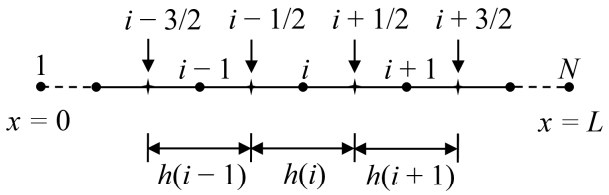

Fig. 10. Numerical mesh used for the finite difference spatial discretization of the 1-D drift-diffusion equation.

Figure 10 shows the numerical mesh that we used for the finite difference spatial discretization of the 1-D drift-diffusion equation.

We approximate the electric field at the half-integer points in the mesh as

$$E_{i+1/2} = -\left(\frac{\psi_{i+1} - \psi_i}{h_i}\right), \tag{26}$$

where ψ_i is the potential at mesh-point i, and we approximate $\partial p/\partial x$ and $\partial n/\partial x$ at the half-integer points as

$$\begin{aligned} \left.\frac{\partial p}{\partial x}\right|_{i+1/2} &= \left(\frac{p_{i+1} - p_i}{h_i}\right), \\ \left.\frac{\partial n}{\partial x}\right|_{i+1/2} &= \left(\frac{n_{i+1} - n_i}{h_i}\right), \end{aligned} \tag{27}$$

where h_i is distance between the points $i - 1/2$ and $i + 1/2$. We calculate the currents at the half-integer points by discretizing Eq. (19) to obtain

$$\begin{aligned} \mathbf{J}_{p,i+1/2} &= q p_{i+1/2} \mathbf{v}_{p,i+1/2}(\mathbf{E}) - q D_{p,i+1/2} \left(\frac{p_{i+1} - p_i}{h_i}\right), \\ \mathbf{J}_{n,i+1/2} &= q n_{i+1/2} \mathbf{v}_{n,i+1/2}(\mathbf{E}) + q D_{n,i+1/2} \left(\frac{n_{i+1} - n_i}{h_i}\right), \end{aligned} \tag{28}$$

where $p_{i+1/2} = (p_{i+1} + p_i)/2$, $n_{i+1/2} = (n_{i+1} + n_i)/2$, $D_{n,i+1/2}$ and $D_{p,i+1/2}$ are the electron and hole diffusion coefficients at the point $i + 1/2$, and $\mathbf{v}_{n,i+1/2}$ and $\mathbf{v}_{p,i+1/2}$ are the electron and hole drift velocities at the point $i + 1/2$. Finally, we approximate

$$\begin{aligned} \frac{\partial \mathbf{J}_{p,i}}{\partial x} &= \frac{\mathbf{J}_{p,i+1/2} - \mathbf{J}_{p,i-1/2}}{[(h_i + h_{i-1})/2]}, \\ \frac{\partial \mathbf{J}_{n,i}}{\partial x} &= \frac{\mathbf{J}_{n,i+1/2} - \mathbf{J}_{n,i-1/2}}{[(h_i + h_{i-1})/2]}. \end{aligned} \tag{29}$$

The total output current is the sum of the electron, hole, and displacement currents and is given by

$$\mathbf{J}_{\text{total}} = \mathbf{J}_n + \mathbf{J}_p + \epsilon \frac{\partial \mathbf{E}}{\partial t}. \tag{30}$$

We use the same model parameters as Hu *et al*. [9]

Funding

Naval Research Laboratory grant number N00173-15-1-G905

Optics EXPRESS

Acknowledgments

A portion of our computational work carried out at the UMBC High Performance Computing Facility (https://hpcf.umbc.edu).
We also want to thank Dr. J. Cahill for his useful comments.

References

1. B. E. A. Saleh and M. C. Teich, *Fundamentals of Photonics* (Wiley, 1991).
2. V. J. Urick, K. J. Williams, and J. D. McKinney, *Fundamentals of Microwave Photonics* (Wiley, 2015).
3. F. Quinlan, T. M. Fortier, H. Jiang, and S. A. Diddams, "Analysis of shot noise in the detection of ultrashort optical pulses," J. Opt. Soc. Am. B **30**, 1775–1785 (2013).
4. R. Paschotta, "Timing jitter and phase noise of mode-locked fiber lasers," Opt. Express **18**, 5041–5054 (2010).
5. S. Wang, T. F. Carruthers, and C. R. Menyuk, "Efficiently modeling the noise performance of short-pulse lasers with a computational implementation of dynamical methods," J. Opt. Soc. Am. B **35**, 2521–2531 (2018).
6. C. R. Menyuk and S. Wang, "Spectral methods for determining the stability and noise performance of passively modelocked lasers," Nanophotonics **5**, 332–350 (2016).
7. F. Quinlan, T. M. Fortier, H. Jiang, A. Hati, C. Nelson, Y. Fu, J. C. Campbell, and S. A. Diddams, "Exploiting shot noise correlations in the photodetection of ultrashort optical pulse trains," Nat. Photonics **7**, 290–293 (2013).
8. W. Sun, F. Quinlan, T. M. Fortier, J. D. Deschenes, Y. Fu, Scott A. Diddams, and J. C. Campbell, "Broadband noise limit in the photodetection of ultralow jitter optical pulses," Phys. Rev. Lett. **113**, 203901 (2014).
9. Y. Hu, B. S. Marks, C. R. Menyuk, V. J. Urick, and K. J. Williams, "Modeling sources of nonlinearity in a simple PIN photodetector," J. Lightw. Technol. **32**, 3710–3720 (2014).
10. Y. Hu, T. F. Carruthers, C. R. Menyuk, M. Hutchinson, V. J. Urick, and K. J. Williams, "Modeling nonlinearity in a modified uni-traveling-carrier (MUTC) photodetector," *IEEE Photonics Conference (IPC)* (IEEE, 2015), pp.122–123.
11. Z. Li, H. Pan, H. Chen, A. Beling, and J. C. Campbell, "High-saturation-current modified uni-traveling-carrier photodiode with cliff layer," IEEE J. Quantum Electron. **46**, 626–632 (2010).
12. H. Ito, S. Kodama, Y. Muramoto, T. Furuta, T. Nagatsuma, and T. Ishibashi, "High-speed and high-output InP-InGaAs unitraveling-carrier photodiodes," IEEE J. Sel. Topics Quantum Electron. **10**, 709–727 (2004).
13. K. J. Williams, R. D. Esman, and M. Dagenais, "Nonlinearities in P-I-N microwave photodetectors," J. Lightw. Technol. **14**, 84–96 (1996).
14. Y. Hu, "Modeling Nonlinearity and Noise in High-Current Photodetectors," Ph.D. Thesis (University of Maryland Baltimore County, 2017).